THE STRAIN MEASUREMENT BY IMAGE PROCESSING TECHNIQUE FOR SHEAR PANEL DAMPER MADE OF LOW YIELD STEEL

Y. Liu*, T. Aoki**

* Graduate student, Dept. of Urban and Environment, Aichi Institute of Technology, Toyota
** Professor, Dept. of Urban and Environment, Aichi Institute of Technology, Toyota

Abstract: In this paper, strain distribution properties of the shear panels under cyclic loading tests are investigated based on image processing techniques. The high precision measurement by the image processing system is confirmed by comparing with the measured value by strain gauges. Various shapes of shear panels are tested and their strain distributions in the panels are obtained. The stress concentration is observed at the corners of the square panels, whereas a square panel with round flares at four corners shows a moderate stress distribution. No stress concentration appears in the panels with vertical stiffeners at both sides. The relationship between shear load – displacement and stress distribution in the panel is unveiled.

Keywords: shear panel damper, image processing technique, strain distribution, repeated loading test, seismic performance.

1. INTRODUCTION

A shear panel damper made of low yield steel has become widely applied to high rise buildings as a hysteretic damper in Japan. This damper is expected to reduce the seismic responses of buildings under strong earthquake loads economically and to improve the energy dissipation capacity (NAKASHIMA and IWAI 1994). But there are few examples used for bridges yet. The shear damper used in buildings causes at most a 5% shear deformation angle, which seems very small compared to rubber bearings generally used in bridges. The deformation capacity of rubber bearings used for bridges reaches 250% in general. Because the shear panel damper made of a low yield steel is advantageous in cost and high durability over rubber bearings. If large deformation capacity is obtained, the shear panel damper may become more utilized for bridges (Yang et al 2007).

The aim of this research is to develop a high seismic performance shear damper. Cyclic loading tests are carried out for square panels with different shaped corners or, with/without vertical stiffeners on both sides. In the cyclic loading test, the crack initiates at four corners of the square shear panel due to the stress concentration, and has grown along with cycles, which decreases steady energy absorption capacity.

In order to clarify the mechanism of the crack initiation of the shear panel damper made of low yield steel, it becomes important to know the strain distribution of the panel. Strain gages are commonly used to measure the strain of the shear panel. But it is difficult to measure up to large-stain range by strain gages. Moreover, because a strain gauge gives the strain value at the point where the strain gage adhered, it is not easy to obtain strain distribution in the whole panel. The image processing technique by using a digital camera has become popular recently (Tateishi and Hanji 2004; Yoshida et al 2003; Sakai and Matsuura 2004; Hosoya et al 2004), by which strain distribution on the whole panel is obtained easily.

This paper describes the development and the application of a new large-strain measurement system by image processing technique. It is validated that the strain measured by the image analysis system is almost equal to the measured value by strain gauges.

2. THE IMAGE PROCESSING TECHNIQUE

Basic knowledge of the measurement by image processing becomes easily obtained by published matters recently. The computer codes of the image measurement system in this study is made by Visual Basic 6.0.

2.1 The flow of the image measurement

The flow from obtaining the image data by digital camera to the calculation of the stress is shown in Fig.1.The red marks are painted on the lower half side of the panel specimen first, as shown in photo.1. Circular marks are put on a white background. The diameter of each mark is about 0.2-0.3mm, and the distance between them is about 5mm.

After these marks are recorded by a high precision digital camera, these points are specified on the imaginary coordinates by the image processing. Finally, strain was calculated by using the two-dimensional Finite Element

Method (2D-FEM) with a constant stress triangular model, where nodal points are coincided with the marks on the imaginary coordinates.

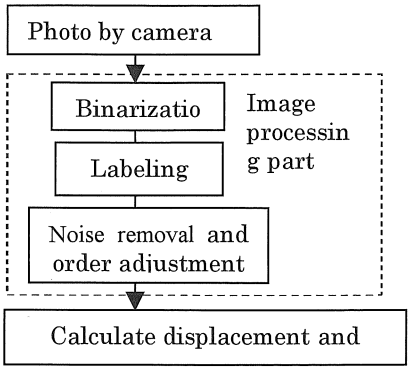

Fig.1 The flow of the image measurement

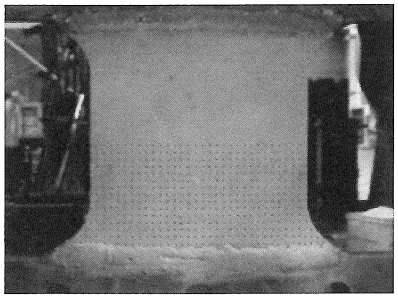

Photo.1 The position of marks

The image processing part in the Fig. 1 is as follows.

(1) Binarization

After setting a suitable threshold value based on color information of the image, each mark and background is binarized to 0 or 1, so that marks could be extracted from the background (Fig.2 (a), (b)).

(2) Labeling

At this stage, a number is put on each mark, and the coordinate of the gravity point of the area, which is the assembly of pixels for each mark, is calculated (Fig.2 (c)).

(3) Noise removal and order adjustment

When the area of a point is recognized to be considerably smaller than others, this point is considered a noise particle and is removed from the image. If a large transformation occurs on the specimen during loading, the regularly arranged mark number is useful in distinguishing them from each other.

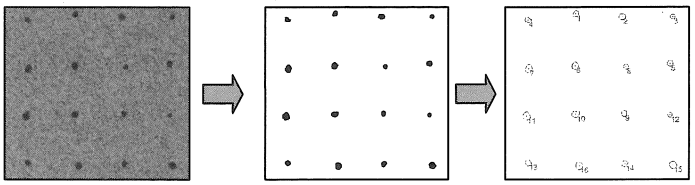

(a) Original image (b) Binarization (c) Labeling

Fig.2 The flow of the image processing

2.2 Calculation of stress

The basic theory of the two-dimensional Finite Element Method (2D-FEM) with a constant stress triangular element is used in the strain calculation. Three points whose coordinates have been obtained by the image processing are designated as i, j, k, as shown in Fig.3. The increment of displacements for each node between two loading steps are written as

$$\{\delta\} = \{u_i \quad v_i \quad u_j \quad v_j \quad u_k \quad v_k\}^T \tag{1}$$

The three strain components are calculated by Eq.(2) together with Eq.(1).

$$\{\varepsilon\} = \langle \varepsilon_x \quad \varepsilon_y \quad \gamma_{xy} \rangle = \left\langle \frac{\partial u}{\partial x} \quad \frac{\partial v}{\partial y} \quad \frac{\partial v}{\partial x} + \frac{\partial u}{\partial y} \right\rangle = \frac{1}{2A} \begin{bmatrix} y_j - y_k & 0 & y_k - y_i & 0 & y_i - y_j & 0 \\ 0 & x_k - x_j & 0 & x_i - x_k & 0 & x_j - x_i \\ x_k - x_j & y_j - y_k & x_i - x_k & y_k - y_i & x_j - x_i & y_i - y_j \end{bmatrix} \{\delta\} \tag{2}$$

where A is area of the triangular element and $x_{i,}$ y_i are the coordinates of the nodal point i.

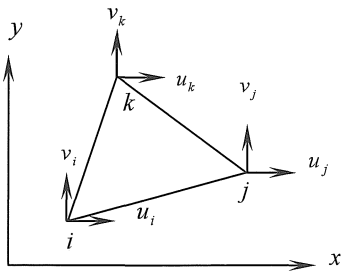

Fig.3 Triangular element

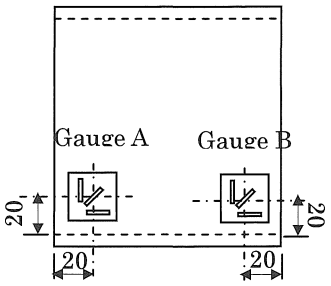

Fig.4 Position of three-axis gauges

2.3 Comparison with results measured by three-axis gauges

Fig.4 shows the position of the gauges put on the plates. The comparison of the shear strain measured by the image analysis system and the three-axis gauges is shown in Fig. 5. The shear strain measured by three-axis strain gauges is calculated by the following equation (3).

$$\gamma = \sqrt{2\left\{(\varepsilon_1 - \varepsilon_3)^2 + (\varepsilon_2 - \varepsilon_3)^2\right\}} \qquad (3)$$

whereε_1, ε_2, ε_3 are the strain obtained by the horizontal, the vertical and the slant direction axis of the three-axis strain gauges, respectively.

Because the adhesive of a strain gauge becomes useless in a large displacement region of the specimen under cyclic loading, the shear strain can only be measured up to 0.05. Within the range of the strain measurement (0-0.05), it is validated that the strain measured by the image analysis system is almost equal to that measured by the strain gauges, as shown in Fig.5.

3. CYCLIC SHEAR TEST OF SEISMIC DAMPERS

3.1 Test specimens, test setup and loading sequence

Before the cyclic loading test, a tensile coupon test is carried out, from which the stress-strain curve is obtained as shown in Fig. 6. The yield strength defined as 0.2% offset value of low-yield steel (LY100) is 80.1 N/mm and elongation reaches 60%, which is about three times that of ordinal structural steel SS400.

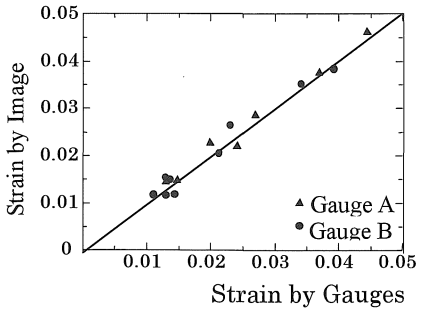

Fig.5 Comparison with the three-axis gauge measurement

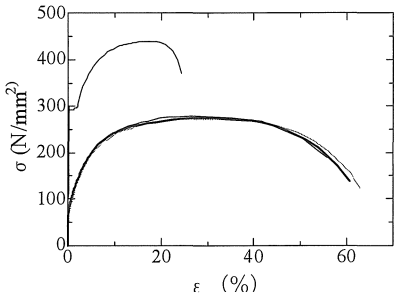

Fig. 6 Stress-strain relationship by tensile test

The shape of the shear panel specimens are shown in Fig.7. Each of the test specimens has a uniform plate thickness of t_w=12mm.

Name and characteristics of four specimens are:

(a) REC: 156×156mm square plate
(b) R3 : with a transition radius R=3 t_w at the four corners
(c) R6.5 : with a transition radius R=6.5t_w at both sides
(d) REC-RIB: with vertical stiffeners along the both sides

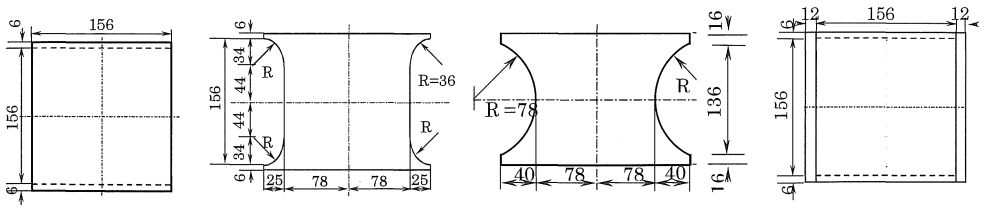

(a) REC (b) R3 (c) R6.5 (d) REC-RIB

Fig.7 Dimensions of specimens (mm)

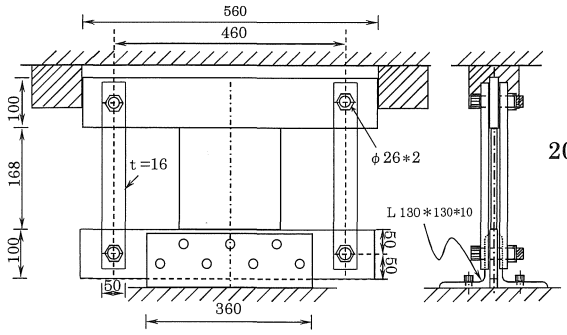

Fig.8 Specimen

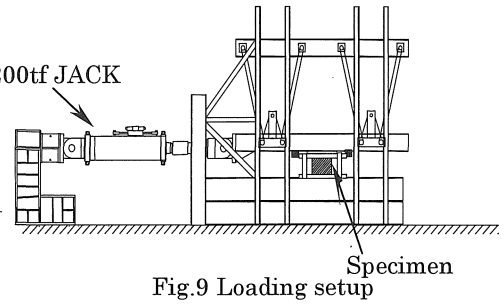

Fig.9 Loading setup

All of the specimens are groove welded to the plates (100 x 360 x 16mm) along the upper and lower edges as shown in Fig.8, and in order that the upper side can move horizontally, the upper plates are connected to lower plate through links. The lower plate are fixed to the base beam with double angles. An overall view of the test setup is shown in Fig.9. The cyclic lateral load was applied at the tip of the upper beam through the W-type leveling apparatus (gravity simulator), that keep the distance between the upper loading beam and the base being constant. The increments of the shear displacement in each loading cycle are $\pm 1\delta_y$, where δ_y= 5mm is the shear yield displacement corresponding to the 0.2% offset yield stress of the material. This displacement history is imposed on the specimens through 5 to 9 cycles up to the displacement where failure occurs.

3.2 Results and discussion

The hysteretic relationship of the normalized shear load (Q/Q_y) to the shear deformation ($\gamma=\delta/H$) for cyclic test specimens is shown in Fig. 10, where Q_y=86.5kN and H=156mm for Specimen REC are used as a common denominator. 1 cycle is equivalent to the shear deformation of 3.2%.

The strain distribution of test specimens at the 3rd cycle is shown in Fig.11, where the vertical axis expresses the Mises equivalent strain calculated by Eq. (4), and the horizontal axis denotes the position of the marks in the panel. These figures show only 1/4 of the specimens.

$$d\bar{\varepsilon}^p = \sqrt{\frac{4}{3}\left((d\varepsilon_x^p)^2 + (d\varepsilon_y^p)^2 + d\varepsilon_x^p d\varepsilon_y^p + \frac{1}{4}(d\gamma_{xy}^p)^2\right)} \qquad (4)$$

where $d\varepsilon_x^p$, $d\varepsilon_y^p$, $d\gamma_{xy}^p$ are the strain increments of x, y directions and shear strain, respectively.

From Fig. 10 and Fig.11 the following are obtained.

(a) Square web plate (REC)

Fig. 10(a) shows the hysteretic curve of shear force versus shear deformation of REC. the Shear load $Q_{max}=2.2Q_y$ and the shear deformation of γ_{max}= 16% (i.e., $\delta=5\delta_y$), which is the lowest in the four specimens, is obtained. The strain distribution of REC is shown in Fig.11 (a). The equivalent strain in the panel corner calculated by Eq. (4) reached 0.17, which is about 5 times the value in the center part. It is clear that the remarkable strain concentration at the panel corners is observed compared with other specimens. Fractures were found at the diagonal corners in the 4th cycle of loading, and progressed with the increasing of horizontal loading that resulted in destruction.

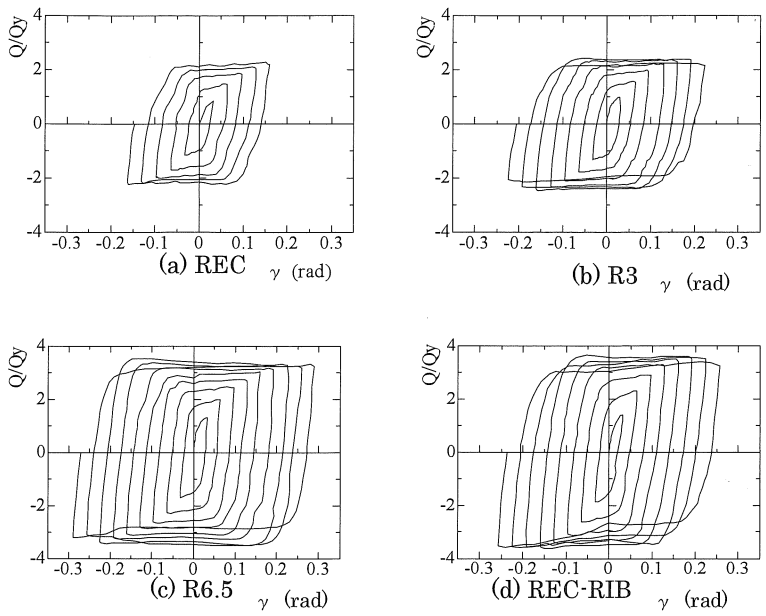

Fig.10 Shear force versus shear deformation relationships

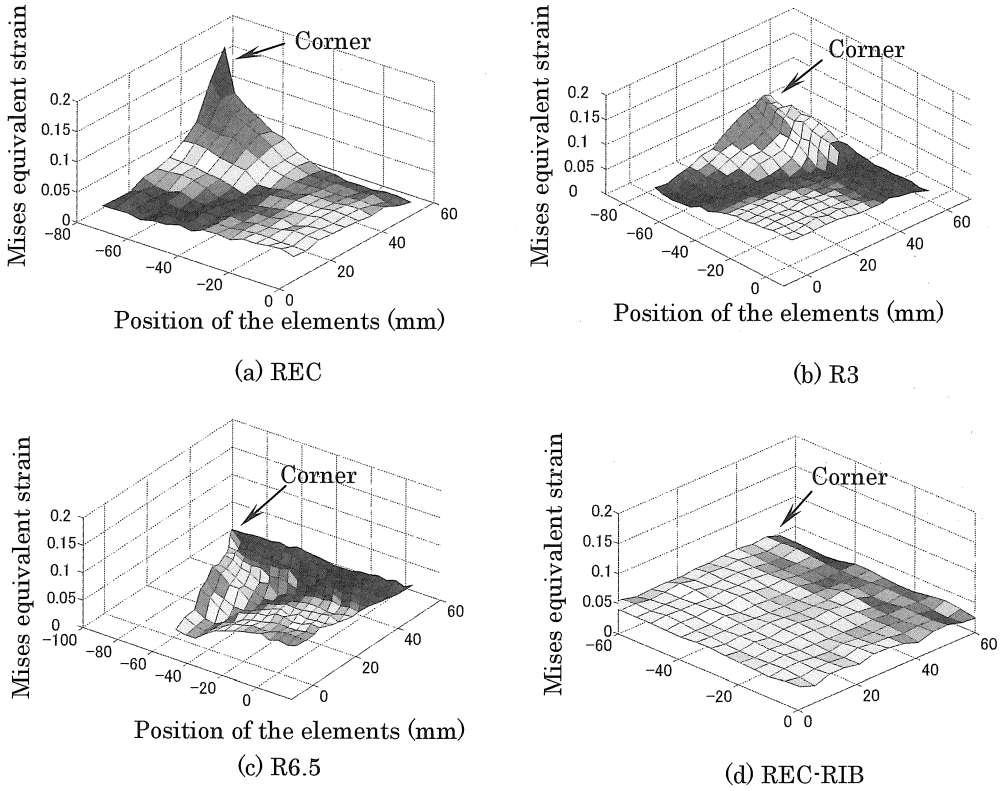

Fig. 11 Strain distribution by image processing

(b) R3

The hysteretic curve of Specimen R3, the shear panel with a transition radius of $R=3t_w=36$mm at the four corners, is shown in Fig.10 (b). From the curve, the shear deformation $\gamma_{max} = 23\%$ (i.e., $\delta = 7\delta_y$) is obtained, increasing 44% than REC, while the maximum shear load $Q_{max}=2.25Q_y$ of R3 is almost the same with REC.

The strain distribution of R3 is shown in Fig.11 (b). Compared with Fig.11 (a), the location of maximum strain moved to the middle part of the arc from the panel corners, and the maximum value was reduced to 0.085 which is about half of that of REC. Moreover, the strain in the region near the center of the panel becomes larger than REC. Therefore, concentration of the strain at the four corners is reduced by the large radius. Reduction of stress concentration

contributes significantly to upgrade the cyclic performance of the shear devices because of delaying fracture initiation at the panel corners.

(c) R6.5

The hysteretic curve of Specimen R6.5, which is a shear panel with a transition radius of R= $6.5t_w$= 78mm, about half of the height, at both sides, is shown in Fig.10 (c).The shear deformation γ_{max} = 28.5% (i.e., $\delta = 9\delta_y$) is the largest of the four specimens provided in the cyclic loading test, and is about 24% larger than R3. As the ductility increases, the maximum shear load Q_{max} of R6.5 increases to $3.3Q_y$, which is about 44% higher than R3.

Fig.11(c) shows the strain distribution of R6.5. Similar to Fig.11 (b), a large strain value appears at the region along the arc of the shear panel. Compared to R3, however, the maximum strain is reduced to 0.073, about 15% down from R3. The strain in the region near the center of the panel shows a larger value than R3. This implies that the relaxation of the concentration of the strain in the four corners leads to a high increase of ductility, and to improve the energy absorption capacity of the shear panel.

(d) REC-RIB

Fig.10 (d) shows the hysteretic curve of Specimen REC-RIB, the shear panel having vertical stiffeners along both edges. Compared to R6.5, the maximum shear load $Q_{max}=2.25Q_y$ is almost the same, but the shear deformation decrease to 25%.

The strain distribution of Specimen REC-RIB is shown in Fig.11 (d). As shown in the Figure, the small strain distributes uniformly in the whole range of the shear panel. The value of the strain only amounts to between 0.035 and 0.045. The crack finally appeared at the bottom of the stiffeners and resulted in the destruction of the specimen.

4. CONCLUSIONS

The main conclusions of this study are:

1. The results of the measurement by the image processing system is compared with the measured value by strain gauges and good agreement is obtained.

2. Measurement of two-dimensional strain distribution of the shear panel damper is very difficult by means of conventional strain gauges. It is found that the image processing system is able to measure easily the strain distribution of the shear panels during cyclic-loading test.

3. Strain concentration generated noticeably at the corners of the rectangular panel REC. The maximum strain at the corner reaches 0.17, that is about 5 times the value in the center part. The shear deformation of γ_{max}= 16% obtained in the test is the lowest of the four specimens.

4. The shear deformation γ_{max} of R3 with four flared corners increase to 23%, which is about 44% larger than REC. The maximum strain of this specimen appears at the middle part of the arc moving from the panel corners. The maximum value is reduced to 0.085 which is about half of that of REC. On the other hand, the strain in the region near the center of the panel becomes larger than REC. It means that the four flared corners make the strain concentration released and balanced.

5. Along with increasing the radius to R=6.5t of the specimen R6.5, the maximum strain was reduced to ε_{max}=0.073 that is 15% down from R3. But the strain in the region near the center became larger than R3. As the ductility increases, the maximum shear load Q_{max} of R6.5 increases to $3.3Q_y$, which is about 44% higher than R3.

6. Setting up stiffeners on the right and left side of the panel produces uniform and very small strain distribution in the panel. The value of the strain only amounts to between 0.035 and 0.045. But because the base of the stiffeners becomes vulnerable at the final cyclic loading stage, the shear deformation decreases to 25%.

5. REFERENCES

Nakashima, M. and Iwai, S. (1994): Energy dissipation behavior of shear panels made of low yield steel, *Int. J. Earthquake Eng., and Structural. Dynamics*, Vol.23, pp.1299-1313.

Yang, L. Mizumo, S. and Aoki, T (2007): Cycle loading tests of shear panel damper made of low yield steel, *J. of Structural Eng., JSCE.*, Vol.53A, No612, pp.560-567.

Tateishi, K. and Hanji, T. (2004): A study on low cycle fatigue strength of welded joints by means of testing system with image analysis, *J. of the Japan society of civil Eng., JSCE.*, No.752/I-66, pp.277-287.

Yoshida, J. and Abe, M. (2003): Mechanical Properties of Lead Measured by the Image Processing Technique, *J. of the Japan society of civil Eng., JSCE.*, No. 724/I-62, 127-139.

Sakai, M. and Matsuura, S. (2004): Strain-Controlled Low Cycle Fatigue Test System with Image-Based Measurement, *Abiko Research Laboratory Rep.* No. U00068.

Hosoya, T., Sakai, H., Uesugi, Y., Yokoo, M. and Kozakura, Y. (2004): A Concrete Segment Measurement System Using CCD Cameras, *J. of the Japan society of civil Eng., JSCE.*, No.751/IV-62, pp.1-11.